Supplemental 1
Field Pin Types

Two examples of unvegetated pins - installed in the center of blowouts of varying sizes. The below pictures are in summer when the vegetation was fully expanded.

Two other examples of the unvegetated pins in winter when plant senesced aboveground around it, but still present, dormant for winter.

The transitional poles were installed on the peripheral edge of blowouts.

The original galvanized steel poles (only installed at the onset in unvegetated blowouts) and fiberglass poles these were replaced with over time and that were used for all three pin types. Multiples are installed because we installed a new pin if an old one was buried or near being buried and each collection recorded the height above the sediment surface of all pins present.

The vegetated pins were installed seaward of blowouts 8m from the crest at set distances. Images below are some examples of the vegetation surrounding these pins in 1 m^2 transects and what a typical install area looked like zoomed out.
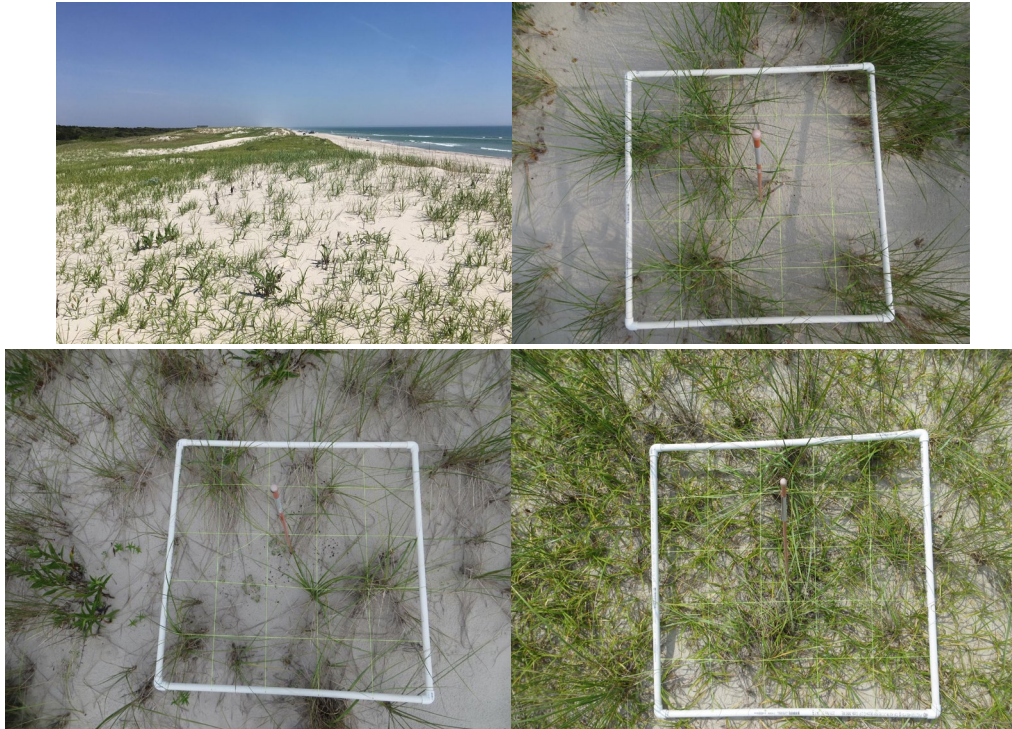
Supplemental 2
Beach & Dune Automated Feature Extraction

This document supplements Section 2.3 from the Methods and pertains to feature extraction from UAS and satellite DEMs for further analysis. Custom tools were built using the Model Builder GUI in ArcGIS Pro v 2.8. DEMs were loaded into the tool and elevations matching the local MHHW line were extracted (Figure S2.1 below). These raster values were converted to points, then lines, which were smoothed to create the georeferenced location of the MHHW which served as the extent of subaerial beach for this study. Results of this tool are presented following the tool description.
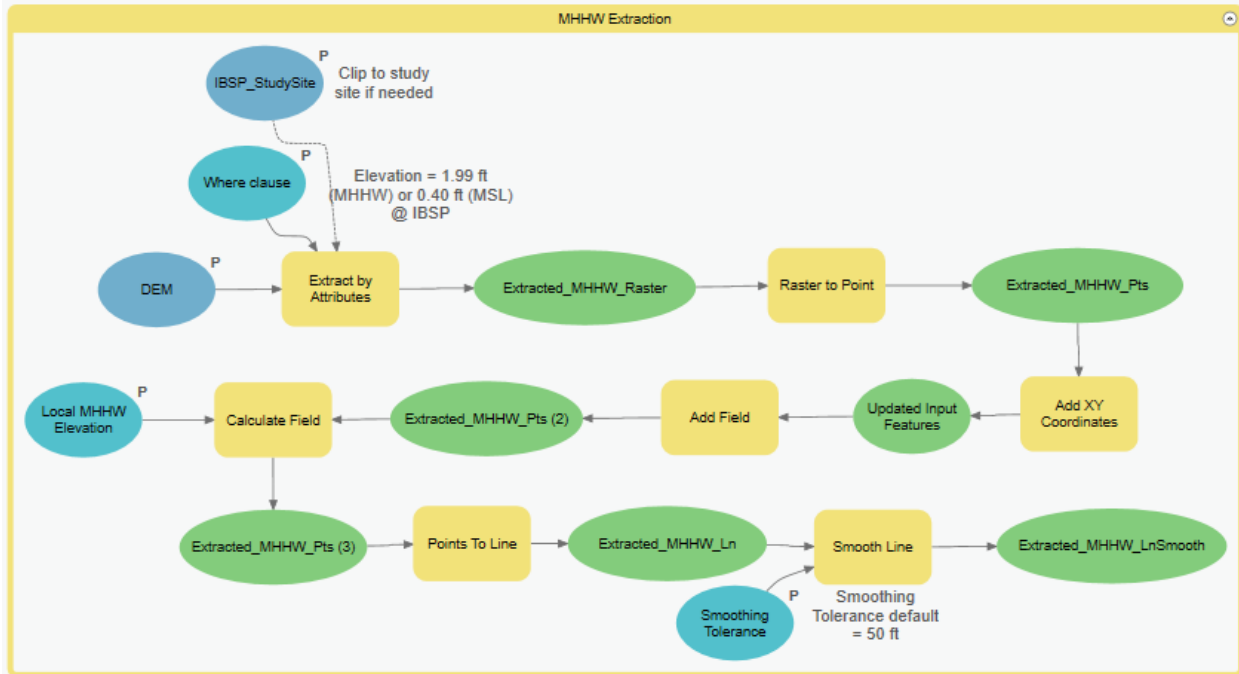
Figure S2.1: ArcGIS Pro model showing how extracted DEMs values created MHHW lines.

Dune crests were extracted using a custom tool built within the Model Builder GUI in ArcGIS Pro v 2.8 (Figure S2.2 below). Curvature surfaces were calculated from input DEMs and then extracted for the maximum positive curvature. This was denoted as the dune crest and agreed well (within 1 m) with the in situ mapping of the crest by the researchers using a Trimble RTK GPS system.
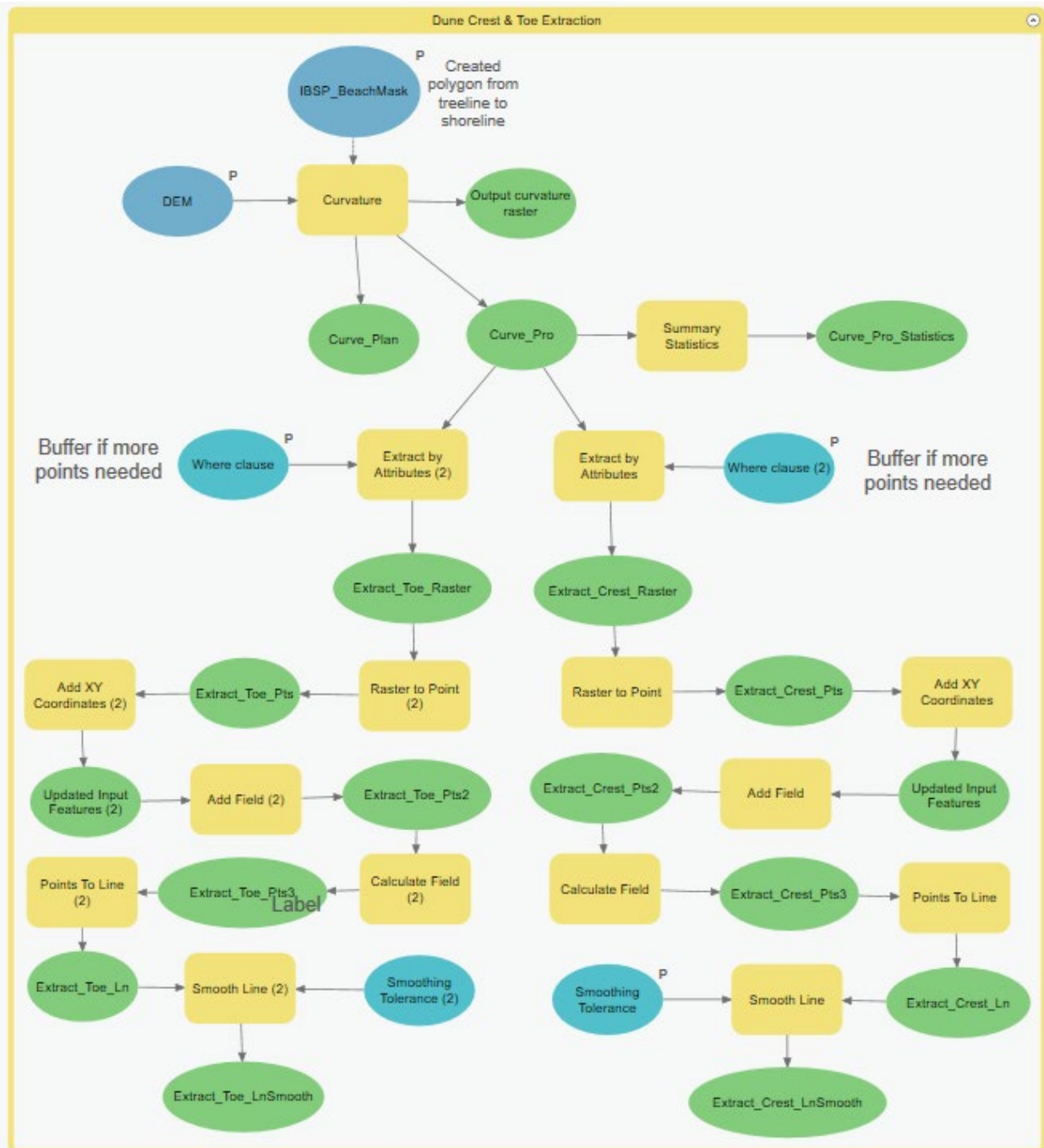
Figure S2.2: ArcGIS Pro model showing how extracted DEMs values created dune crest lines.

Beach widths were calculated using a custom tool built within the Model Builder GUI in ArcGIS Pro v 2.8 (Figure S2.3 below). The extracted dune crests and MHHW lines were used to denote the extent of the subaerial beach as these areas would be most consistently exposed to aeolian processes rather than swash zone dynamics.

```
Widths were calculated for 2014 (72 ± 255 m), 2017−03 (61 ± 393 m),
2017−12 (79 ± 33 m), and 2018−04 (63 ± 150 m).
```
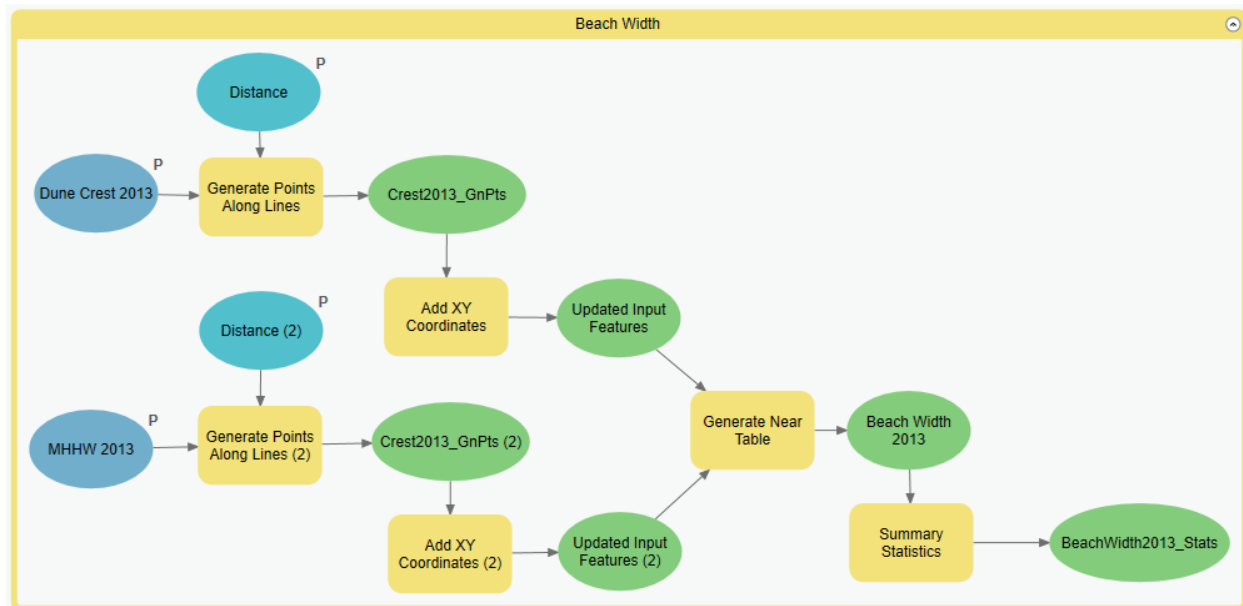

Figure S2.3: ArcGIS Pro model showing how extracted DEMs values contributed to beach width calculations.

Using the tool described above, the crests and MHHW lines were extracted from lidar and UAS surveys from 2014 to Apr 2018. One crest was mapped in situ using a Trimble RTK GPS system following extratropical cyclone Jonas in January 2016. See Table 2 for details of survey dates and sensors. Crests showed more variability near Accesses 23 and 24 near the southern extent of the collection area. Access 24 is a surf-fishing vehicle path and Access 23 is located directly in front of a large parking lot. Variability in crest location occurred consistently near beach access path crest terminations. This is expected as the crest is discontinued due to the access paths breaking up the crest and causing a disruption to what would normally be a continuous dune crest. These locations are responsible for the larger beach width values within the statistics presented in section 3.1 of the main manuscript.
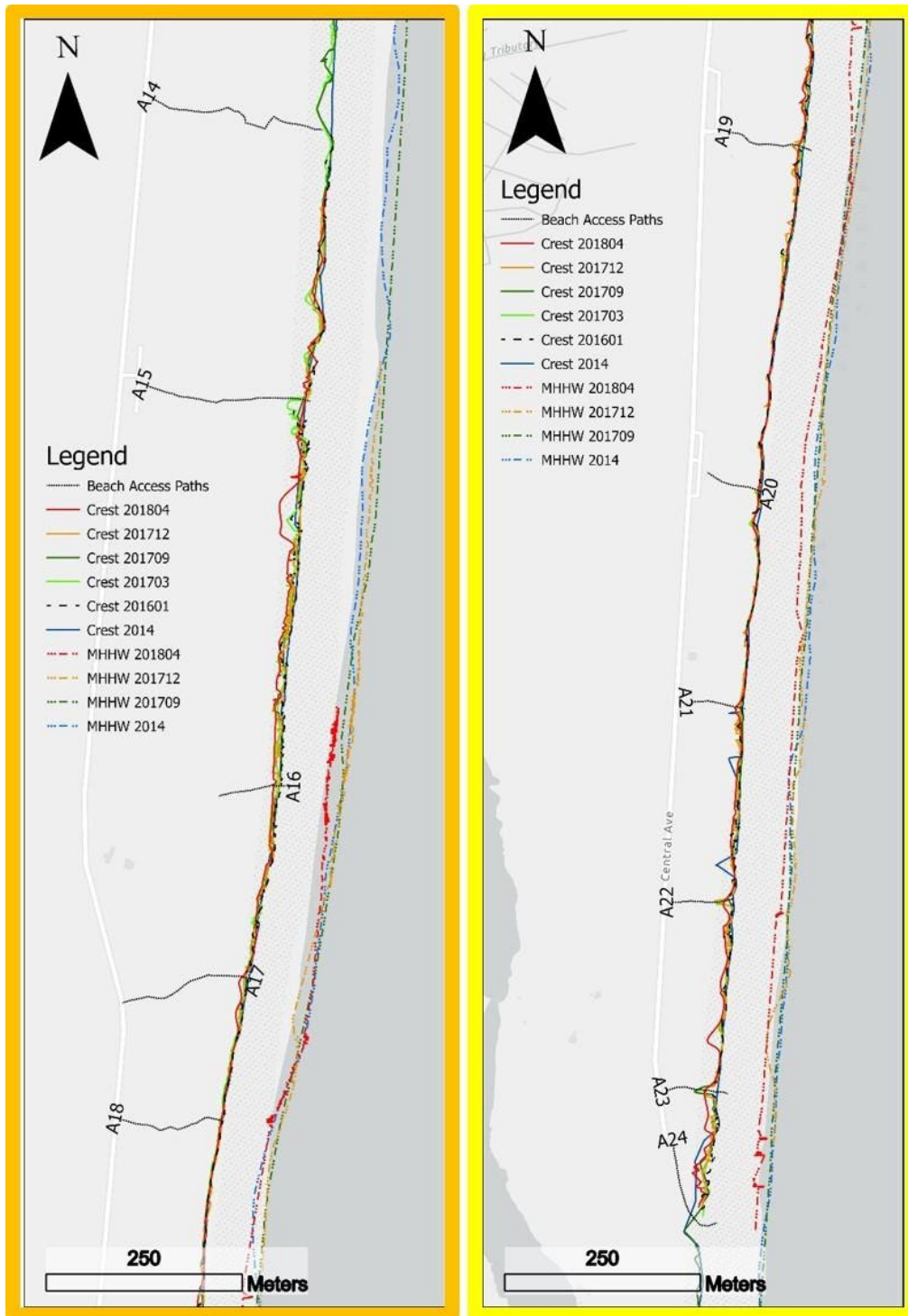
Figure S2.4: Extracted crests and MHHW locations from 2014 - 2018 using a combination of UAS and lidar DEMs with *in situ* RTK GPS mapping. The left figure (orange) shows the northern half of the collection area while the right (yellow) shows the southern half.

Supplemental 3
Beach Access Path Impacts Tool

Below is a walkthrough of the steps used in ArcGIS Pro to quantify the impacts of the beach access paths on the neighboring elevation change at the mesoscale. This custom tool is shown below in Figure S3.2.

1. User inputs the following datasets: access paths shapefile, standard deviation raster, elevation difference raster, path buffer distance (default is 12.2 m or 40 ft on both sides of the mapped path line), and file save path.
    a. Elevation difference rasters were created using two DEMs and the Minus tool.
    b. Standard Deviation rasters utilized the elevation difference rasters created above and the Focal Statistics tool (Figure S3.1). The annulus shape was used with a 1 to 3 raster cell ratio between the inner and outer circles.

Figure S3.1: Example of standard deviation surface created with the Focal Statistics tool. Areas in black are greater than one standard deviation of the mean surface elevation change for 2014-2017. Areas less than one standard deviation are transparent.

2. If the shapefile doesn't exist, the tool creates the path buffer shapefile based on the user inputed distance then extracts the corresponding areas between the standard deviation raster and the buffer shapefile (this work used a mask for the maritime forest, thus it was not included in the analysis).
    a. Masks for the collection area were created using a satellite orthoimage from 2015 during the growing season. The image was converted to an NDVI raster then any areas with a value greater than 0.40 (denoting maritime forest) were extracted and

converted to a polygon. This polygon was clipped to the collection area northern and southern extents then to the shoreline and main road to the east and west.

3. The extracted standard deviation raster is converted to an integer raster. This raster is then extracted by attributes for values greater than zero.

4. Remaining values are converted from a raster to a polygon then polygons are aggregated (based on the surface resolution, here it was 6.1 m or 20 ft with a minimum area of 0.93 m^2 or 10 ft^2).

5. The Minimum Bounding Geometry (Convex Hull option) tool is used to calculate the spatial parameters of each polygon and exported to a shapefile and attribute table.

6. The user inputted elevation change raster is summed for the polygon areas using the Summarize Within tool.

7. Using these sums, the polygon attribute table is updated with the categorical elevation change (erosion or accretion) based on the sign of the sum.

8. The attribute table is manually updated with the nearest access path number and the polygon location along the access path. Crest denotes that the polygon intersects the dune crest. Head corresponds to polygons intersecting with the start of the path at the most inland point. Middle includes any polygons not identified as Crest or Head.

9. Finally, the attribute table is exported to the user inputted file path.

Figure S3.2: Custom access impacts tool in ArcGIS Pro created using the Model Builder module.

Appendix 4

Grain Size Distributions & Analyses

This document supplements Section 2.4 from the Methods and pertains to sediment sample collection, processing, and statistical grain size analysis. 58 push cores were collected in the summer of 2018 using a T soil core sampler (Figure S4.1). 1 m cores were collected on the foredune at 31 locations corresponding to vegetated elevation pin installments. Half meter cores were collected at 20 locations along the dune toe, in alignment with corresponding vegetation elevations pins.
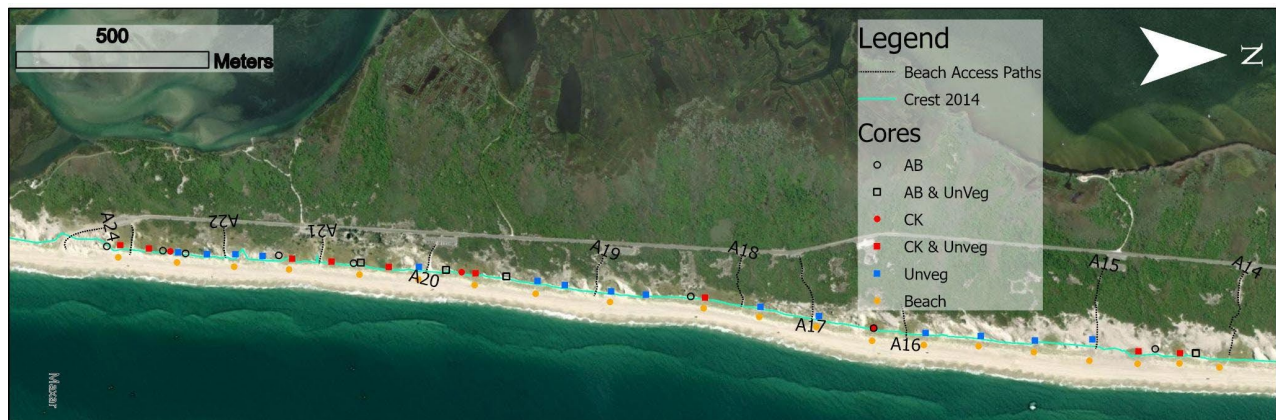
Figure S4.2: Locations of sediment cores taken at the study site in 2018.

Each sample was dried, then sorted for 5-minutes in a RX-29 Ro-Tap cascade shaker using eight different US Standard Sieve Mesh Sizes, mesh #25 (0.71 mm, ϕ 0.5), #35 (0.50 mm, ϕ 1.0), #45 (0.35 mm, ϕ 1.5), #60 (0.25 mm, ϕ 2.0), #70 (0.21 mm, ϕ 2.25), #100 (0.149 mm, ϕ 2.75), #140 (0.105 mm, ϕ 3.25), and the bottom pan (<0.105 mm, ϕ >3.25). Raw sieve weights for each sample were processed using the MATLAB open-source code, SANDY (Ruiz-Martinez et al. 2016). Figure S4.2 below shows all *d50* values (top bar plot) for the cores at all locations and the bottom table summarizes the sorting, skewness, kurtosis, and sediment source values for all cores, vegetated (taken among monocultures of native *Ammophila breviligulata* (AB) or invasive *Carex kobomugi* (CK)), Beach (dune toe), and unvegetated (blowouts) elevation pins.

Bar plot titled "All Cores: d50", y-axis D_{50} [mm], x-axis sample.
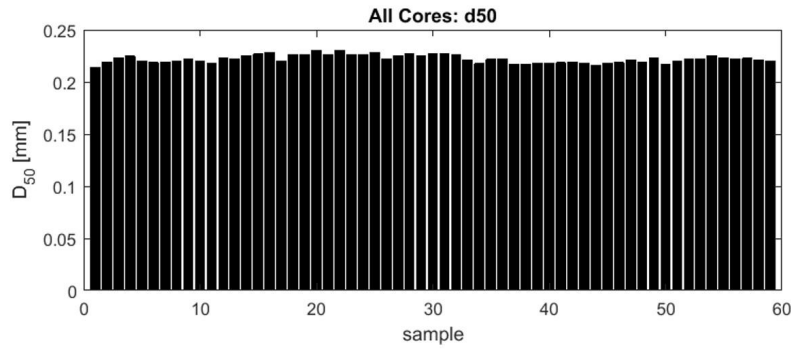
	All	AB	CK	Beach	Unveg
d_{50} [mm]	0.22 ± 0.004	0.22 ± 0.002	0.22 ± 0.003	0.23 ± 0.003	0.22 ± 0.002
Sorting	Very well sorted	Very well sorted	Very well sorted	Very well sorted	Very well sorted
Skewness	< 0	< 0	< 0	< 0	< 0
Kurtosis	Very platykurtic	Very platykurtic	Very platykurtic	Very platykurtic	Very platykurtic
Deposition Environment	Aeolian, Shallow Marine	Aeolian, Shallow Marine	Aeolian, Shallow Marine	Aeolian, Shallow Marine	Aeolian, Shallow Marine

Figure S4.2: Bar plot (top) of *d50* values for all sediment samples from the 2018 collection. A summary statistics table (bottom) splits the sediment samples based on the vegetation type (AB & CK) and location (Beach & Unvegetated). The first column describes all the available sediment samples.

All samples were very well sorted with sorting values 1 ± 0.006 mm (Figure S4.3). Skewness values for all samples had a median value of -0.215 ± 0.039 (Figure S4.4). Therefore all samples were skewed towards coarser grains with a skewness value less than zero. Kurtosis values for all samples had a median value of 0.643 ± 0.015 (Figure S4.5). Thus all samples were very platykurtic (kurtosis < 0.67). Depositional environment was determined using Sahu (1964) methods (Figure S4.6) and demonstrated that all samples were aeolian and shallow marine environments.
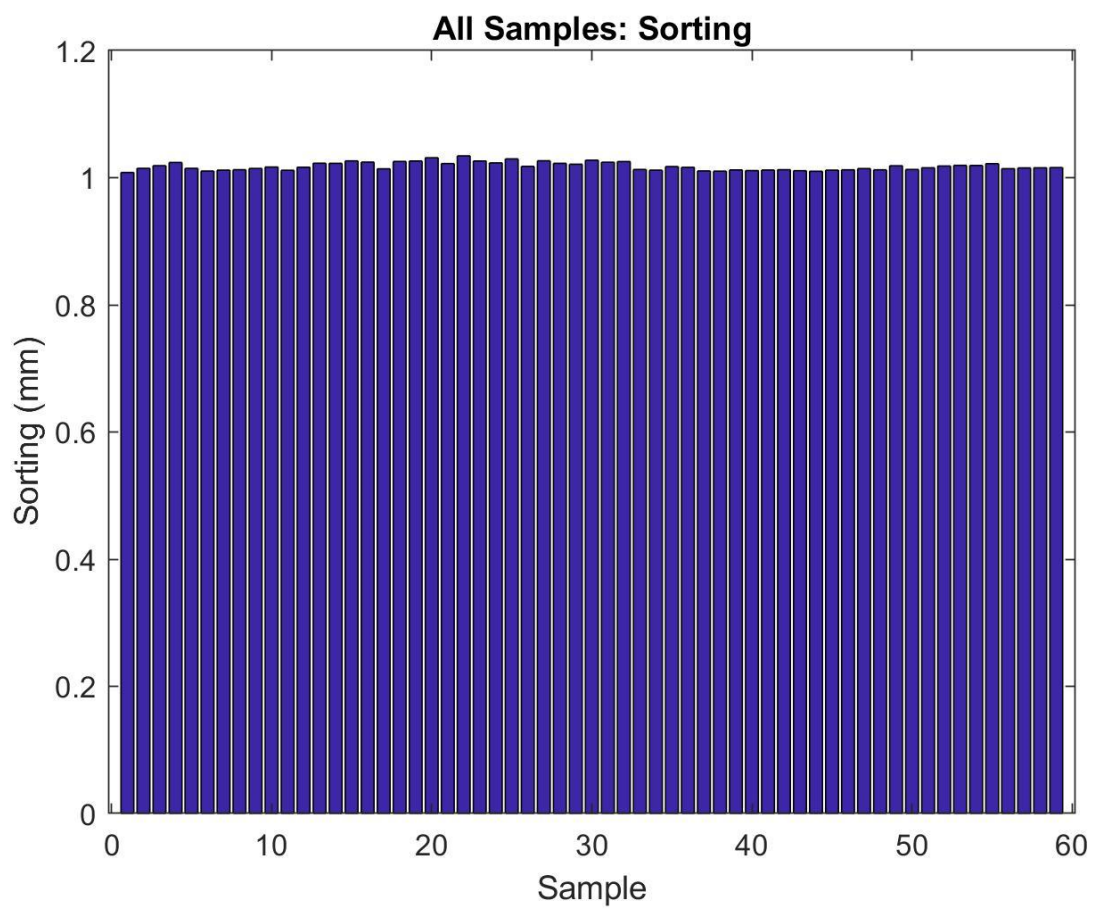
Figure S4.3: Sorting for all sediment samples taken in 2018.
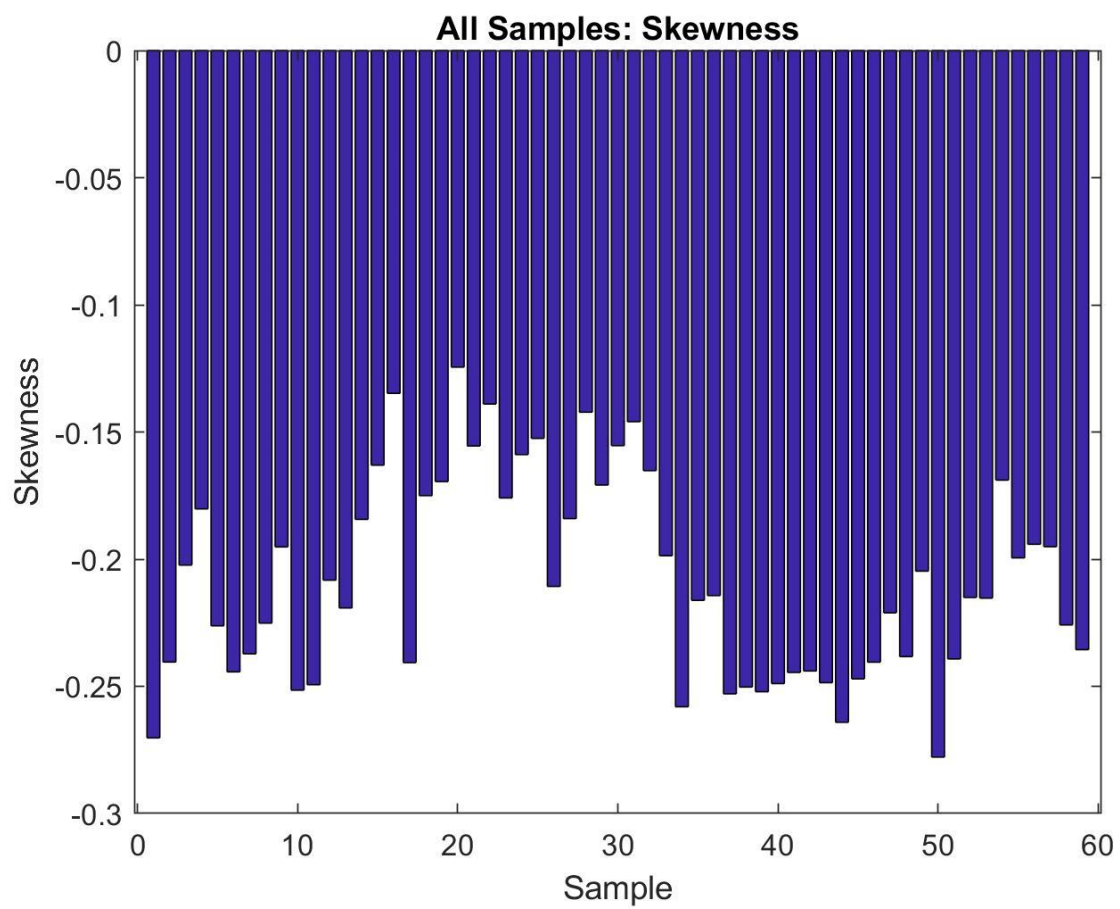
Figure S4.4: Skewness for all sediment samples taken in 2018.
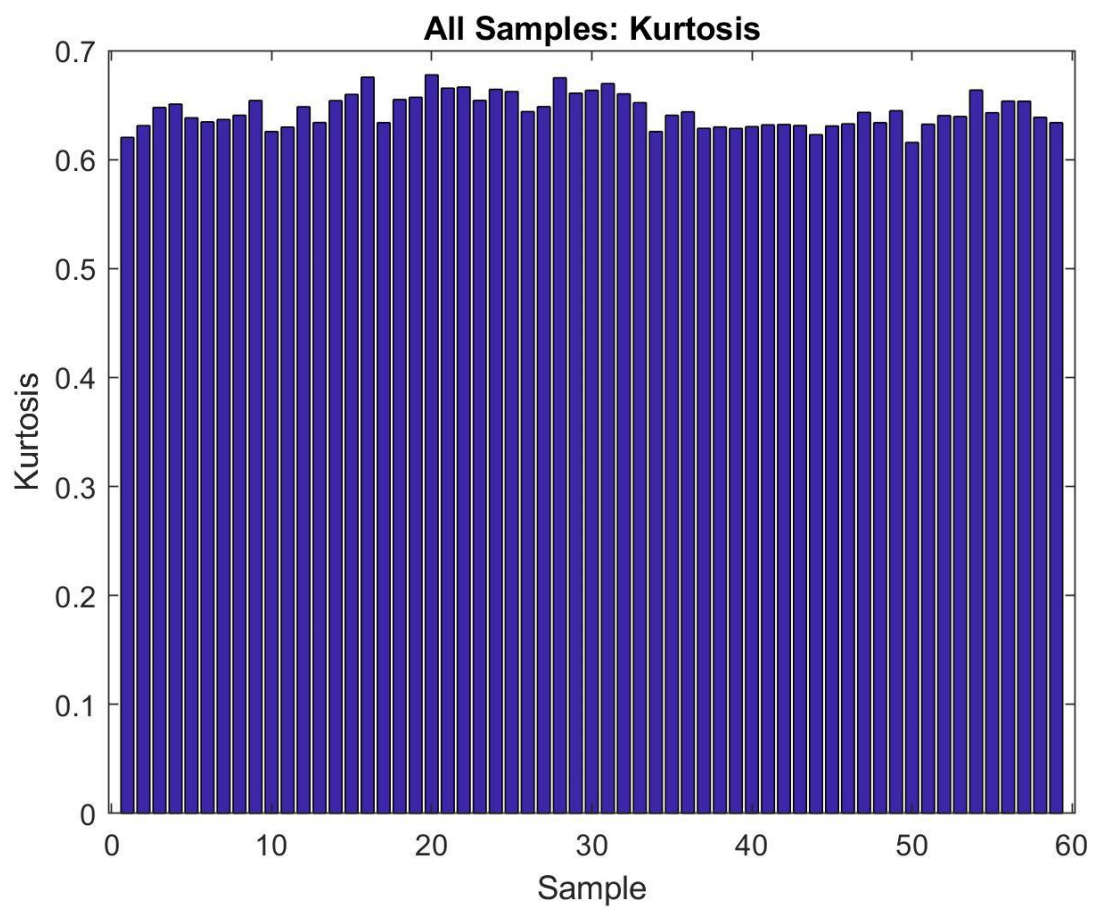
Figure S4.5: Kurtosis for all sediment samples taken in 2018.
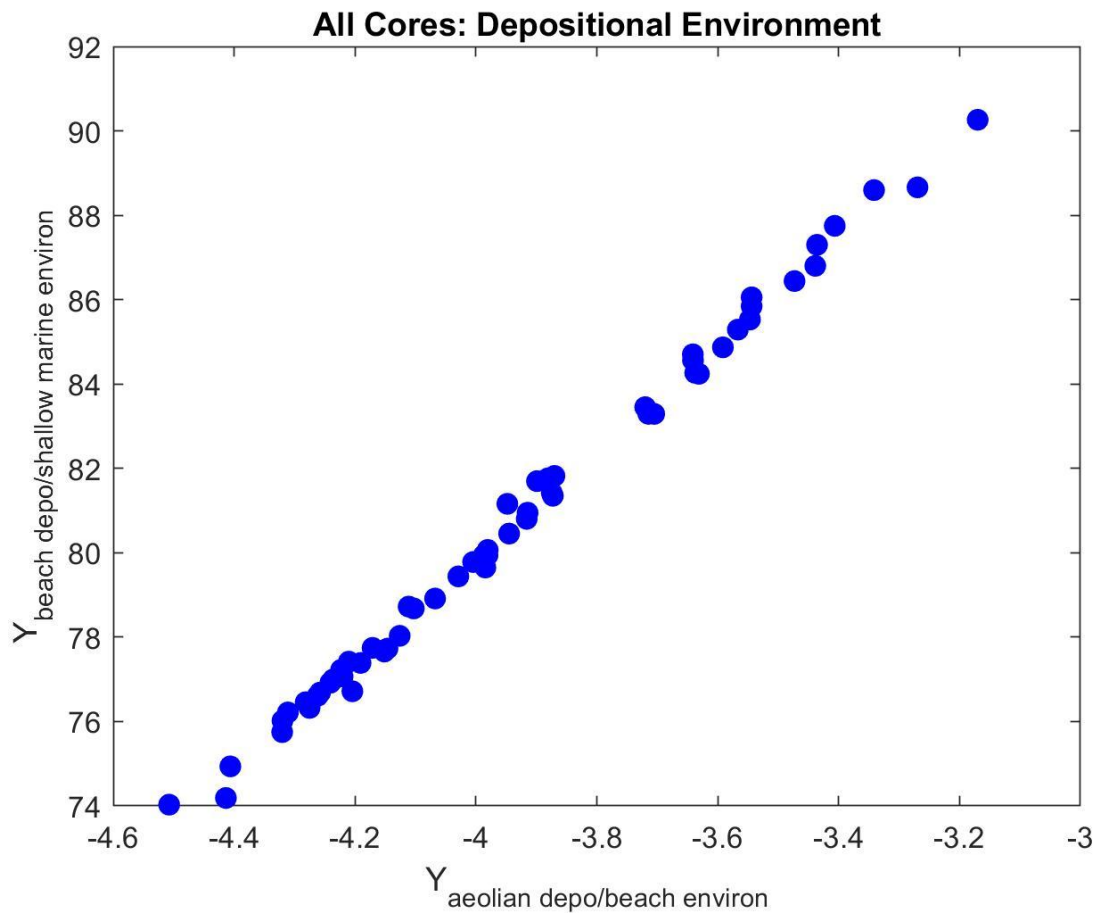
Figure S4.6: Depositional environment for all sediment samples taken in 2018.

Supplemental 5
Meteorological Data & Associated Wind Roses

The specific info on the four stations used can be found online as part of the NJ Rutgers Weather Network. The main station used is Seaside Heights, the data of which was supplemented with Harvey Cedar or Sea Girt station data during any sensor outages.

- Harvey Cedars (HC) - https://www.njweather.org/station/316
  - Wind sensor height = 11 m
- Seaside Heights (SSH) - https://www.njweather.org/station/298
  - Wind sensor height = 12 m
- Sea Girt (SG) - https://www.njweather.org/station/287
  - Wind sensor height = 10 m

Dates of use for the different stations are:

- SSH 1/1/15 0:00 to 2/26/15 23:55
- HC 2/27/15 0:00 to 4/13/15 11:30
- SG 4/13/15 11:35 to 5/14/15 1:25
- SSH 5/14/15 1:30 to 5/11/16 0:00
- HC 5/11/16 0:05 to 11/14/16 11:55
- SSH 11/14/16 12:00 to 9/22/18 0:00

Methods:

1. Data tagged for site, season, & period between field measurements.
2. Data for each station was corrected from sensor height to surface level using von Karman 'law of the wall' equation. Uncorrected for beach slope, humidity, sediment moisture, temperature, or pressure (Equations 1 & 2 from the manuscript).
3. Critical velocity for threshold of motion determined using Shields equation for quartz sand (Equation 3 from the manuscript).
4. Surface velocities plotted in polar format (rose plots) for all available years (Figure S5.1), critical mobility thresholds (Figure S5.3), annual (Figure S5.4), season (Figure S5.5), and periods between field measurements. Additional figure shows the time series for surface velocities and precipitation for 2015 - 2018 (Figure S5.2).

General wind conditions (speed and direction) 2015 to 2018
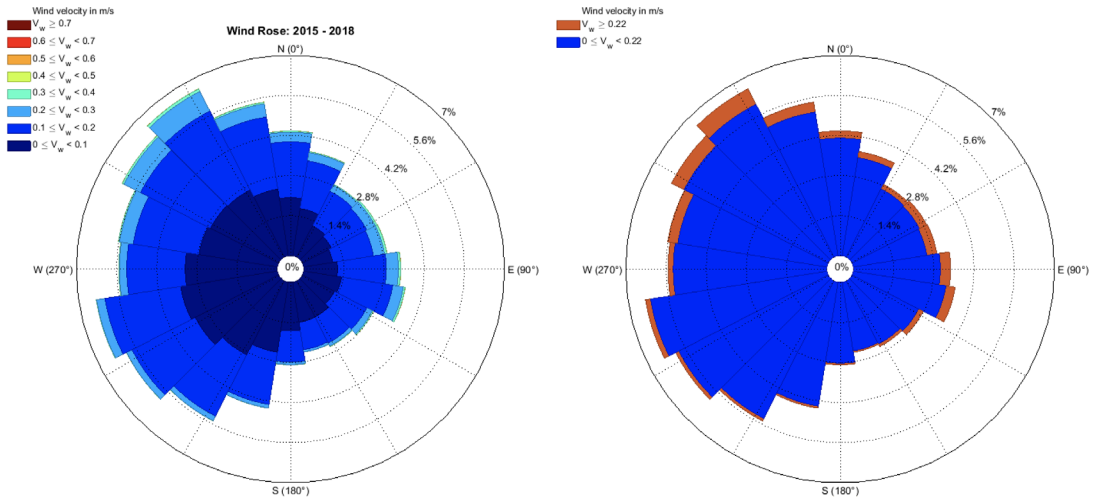
Figure S5.1: All surface wind velocities from 2015 - 2018 (left). All surface wind velocities and directions from 2015 -2018 color coded for above (orange) and below (blue) the Shields critical threshold velocity for mobility (right).
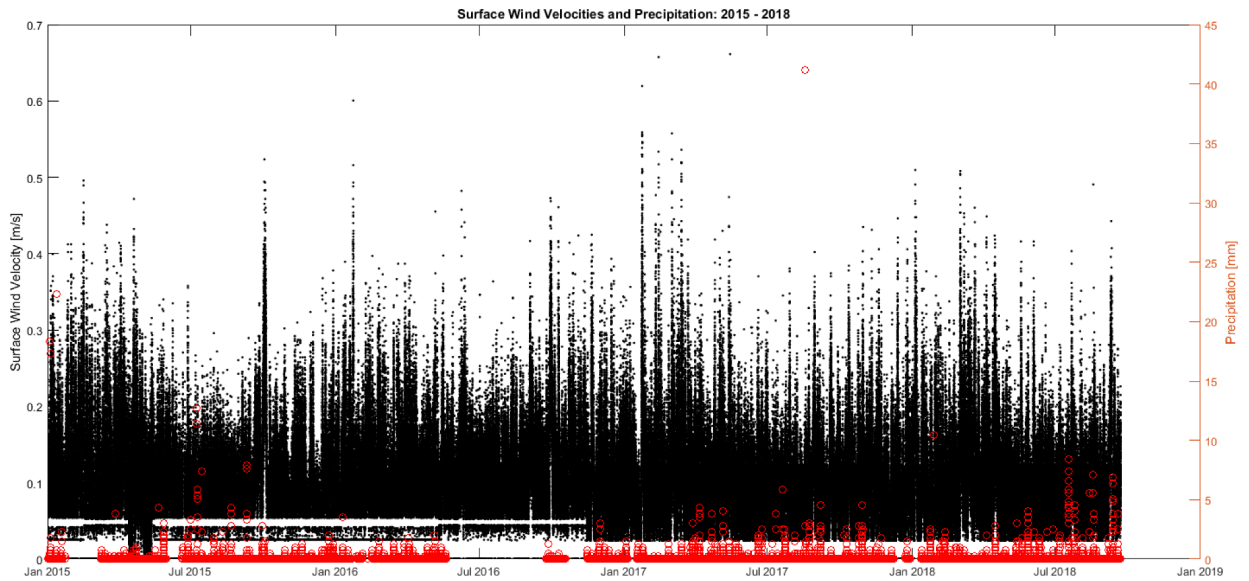
Figure S5.2: All surface wind speeds (black dots, m/s) and precipitation amounts (red circles, mm) from 2015 - 2018.
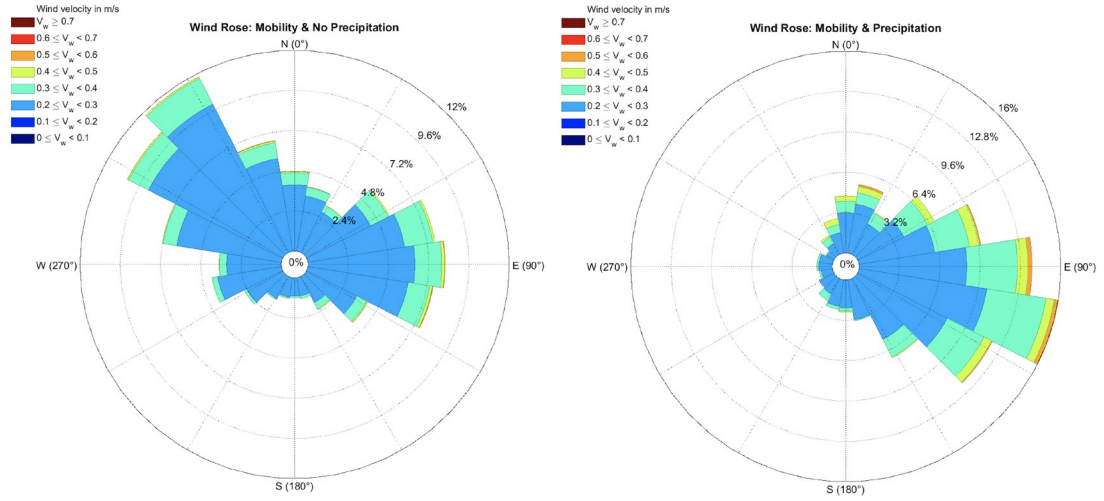
Figure S5.3: All wind velocities greater than the critical mobility velocity corresponding to instances of no precipitation from 2015 -2018 (left). All wind velocities greater than the critical mobility velocity corresponding to instances of precipitation from 2015 - 2018.
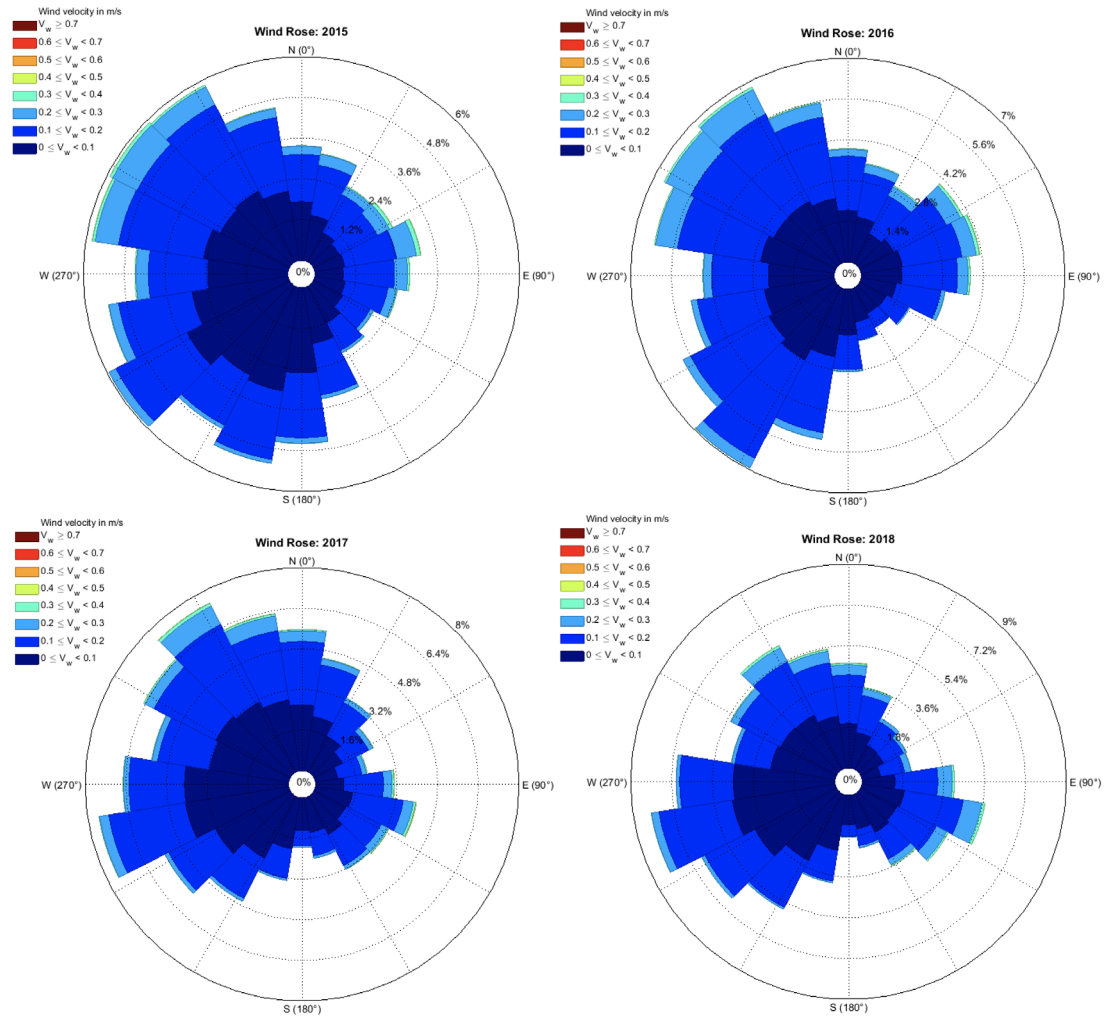
Figure S5.4: Annual surface wind velocities. Scale values are consistent across the polar plots, only the frequency bands differ between plots.

Wind conditions (speed and direction) between seasons.
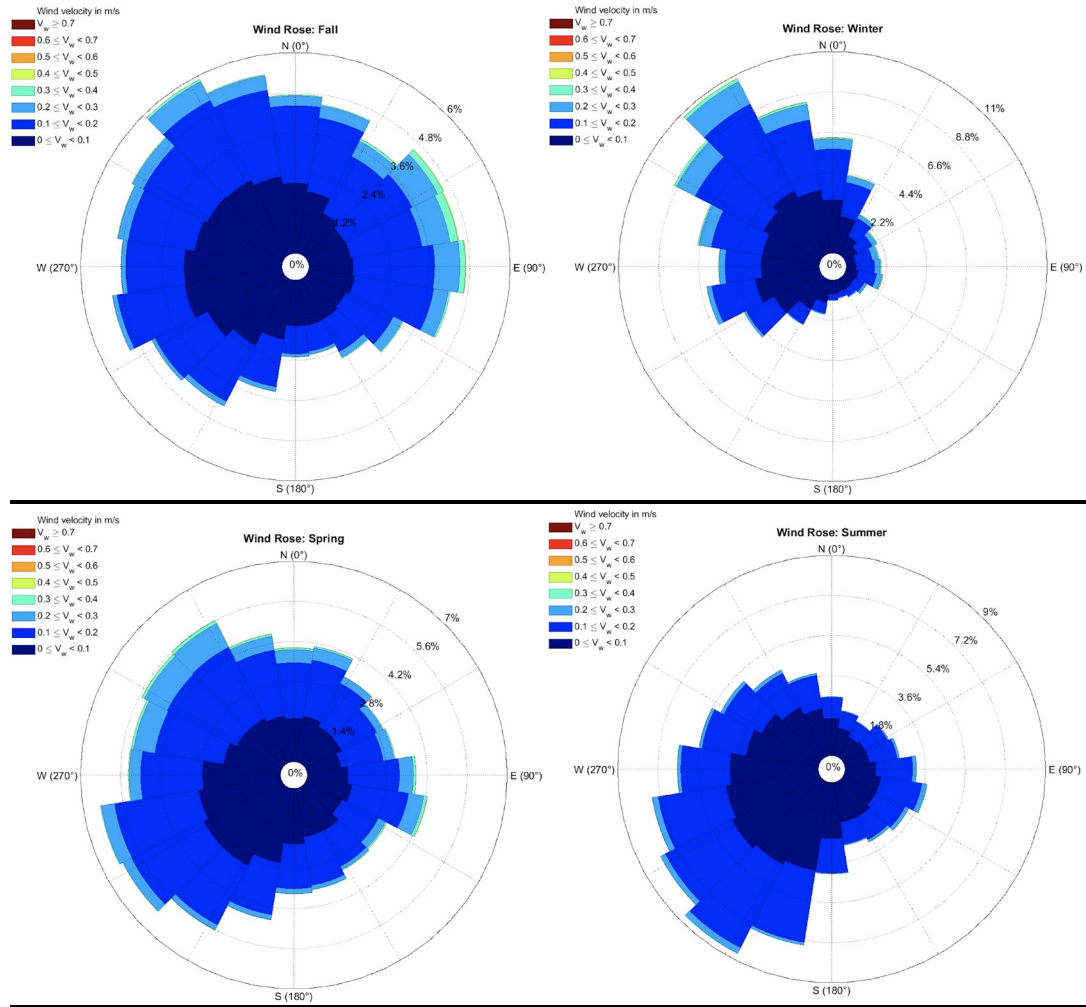
Figure S5.5: Seasonal (2015 - 2018) surface wind velocities. Fall corresponds to the months of September -November; Winter corresponds to December - February; Spring represents March - May; Summer represents June - August. Scale values are consistent across the polar plots, only the frequency bands differ between plots.

Wind conditions (speed and direction) between collections, per period.

Boxed period titles are those during which there was a wind-event. All wind roses are subject to the same categorizations for colors relating to wind velocity in m/s as denoted in the overarching key.

Wind velocity in m/s

- $V_w \geq 0.7$
- $0.6 \leq V_w < 0.7$
- $0.5 \leq V_w < 0.6$
- $0.4 \leq V_w < 0.5$
- $0.3 \leq V_w < 0.4$
- $0.2 \leq V_w < 0.3$
- $0.1 \leq V_w < 0.2$
- $0 \leq V_w < 0.1$
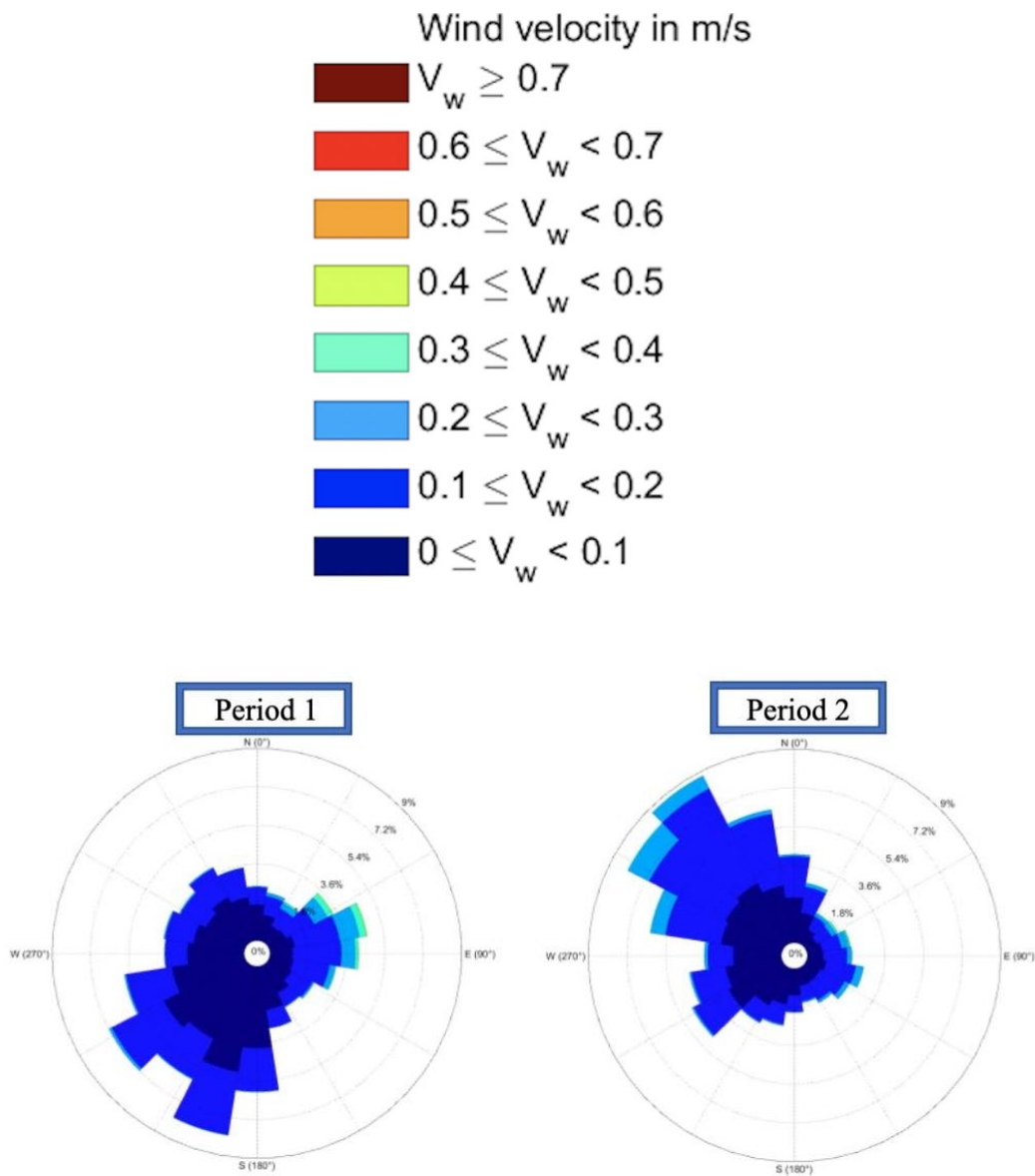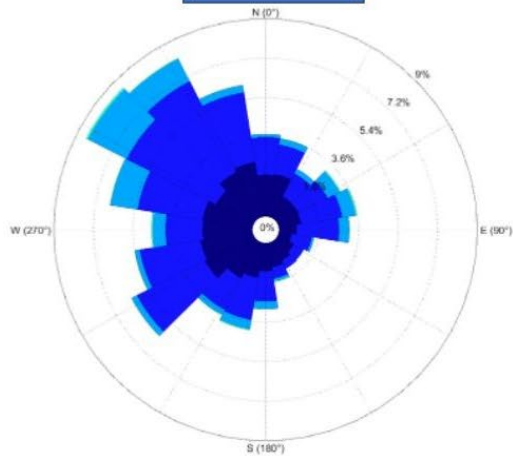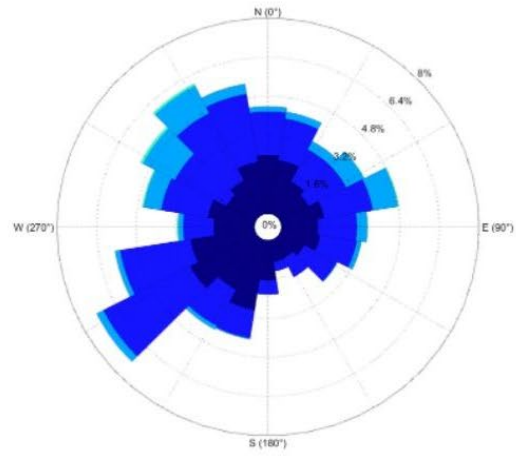
Period 3

Period 4

Period 5
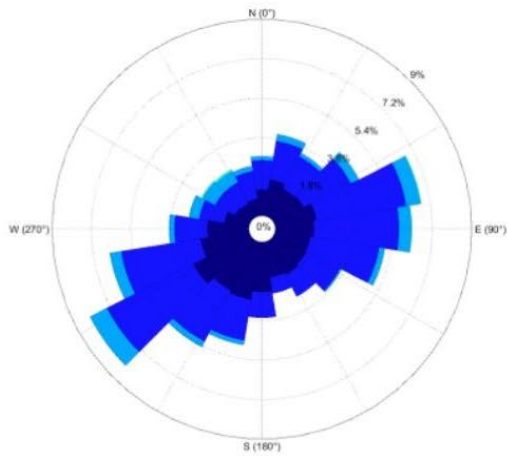
Period 6
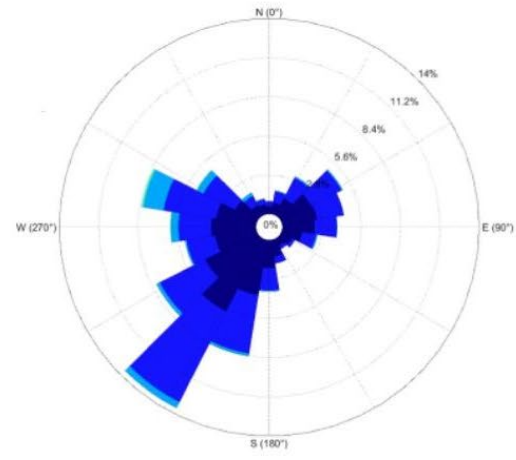
Period 7
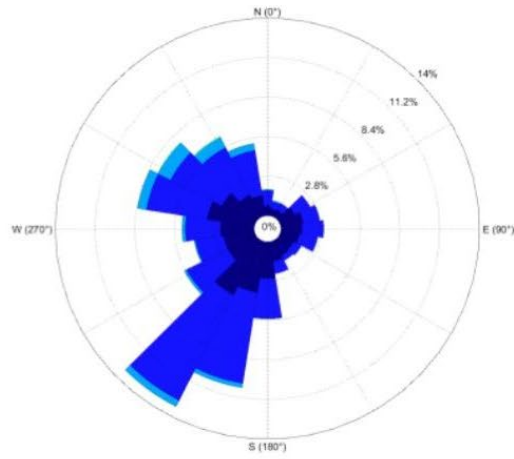
Period 8
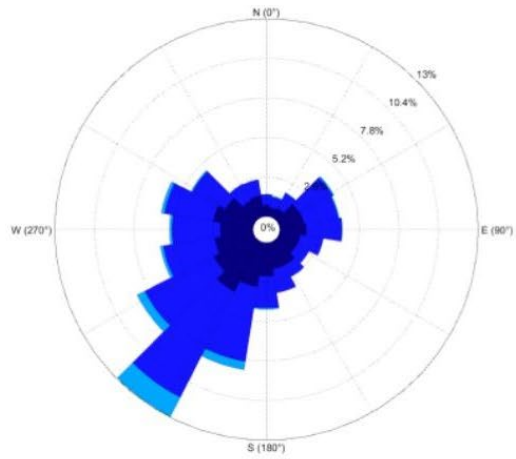
Period 9
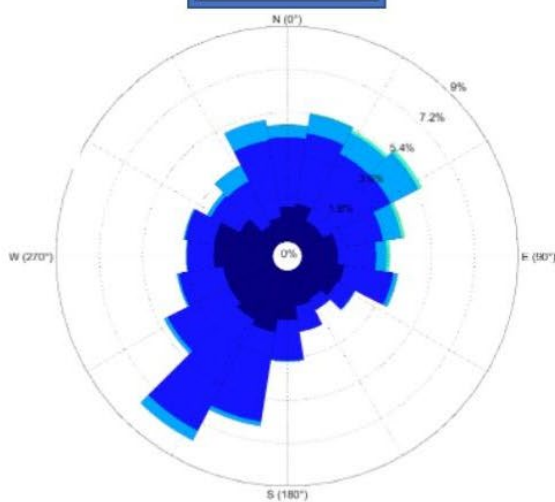
Period 10
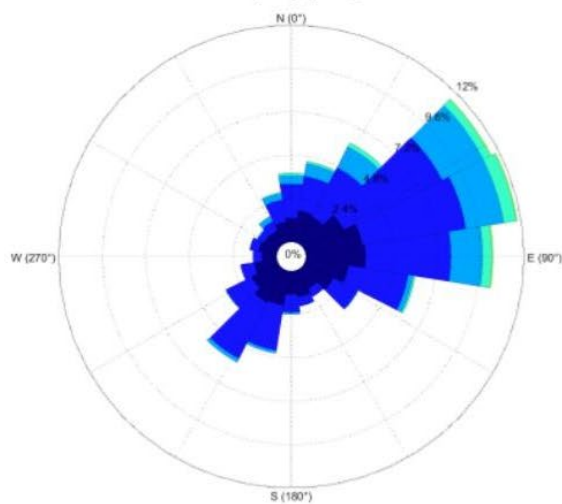
Period 11
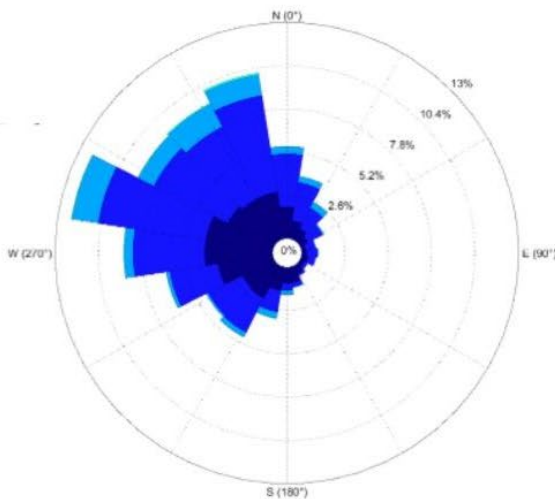
Period 12
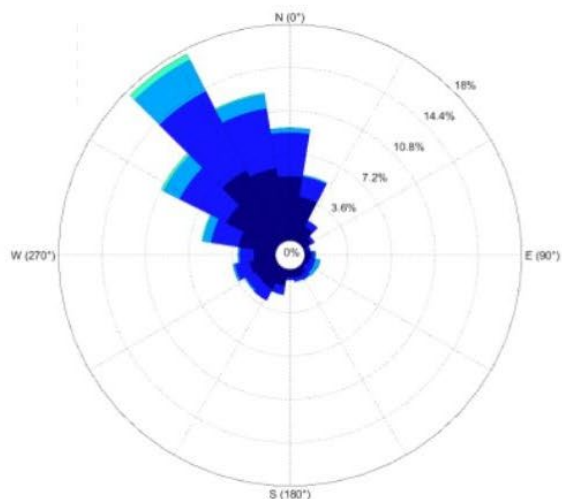
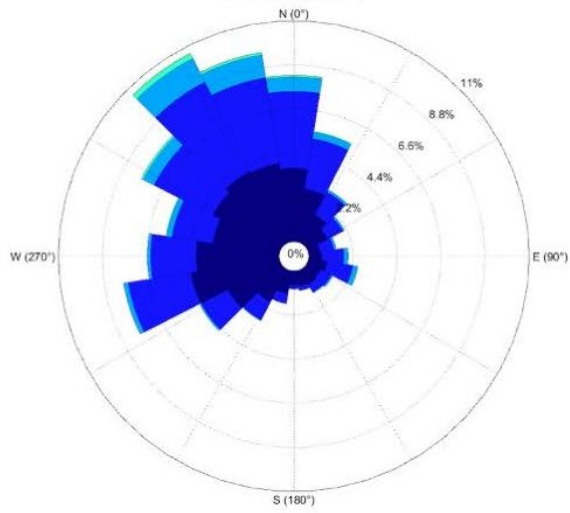Period 13
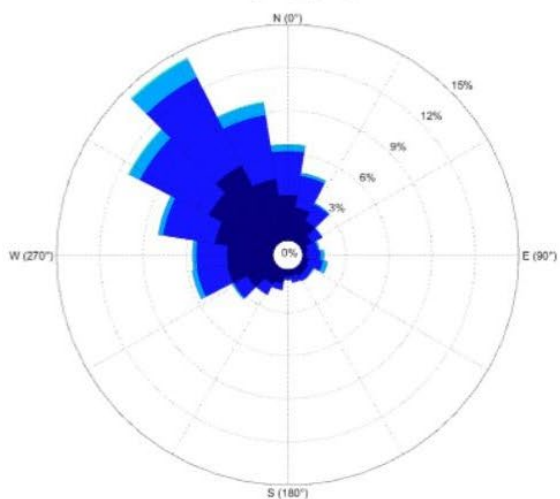
Period 14
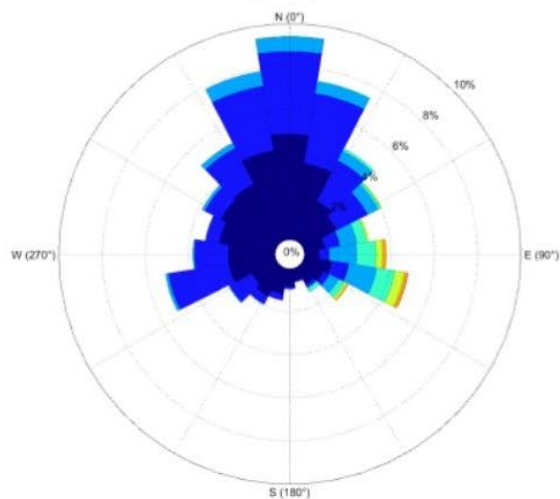
Period 15
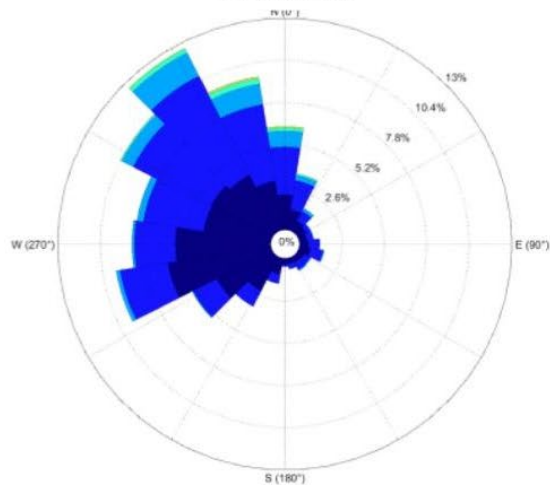
Period 16
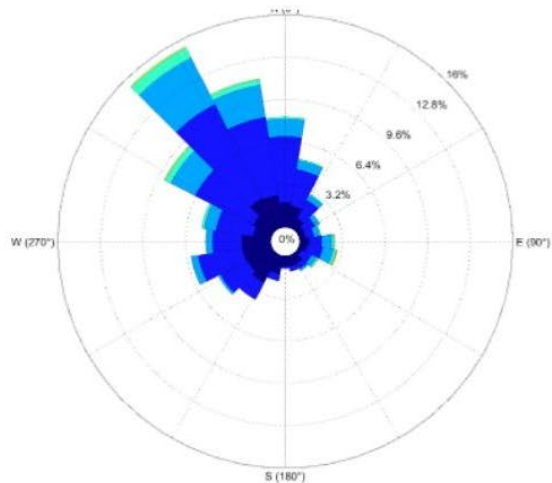
Period 17
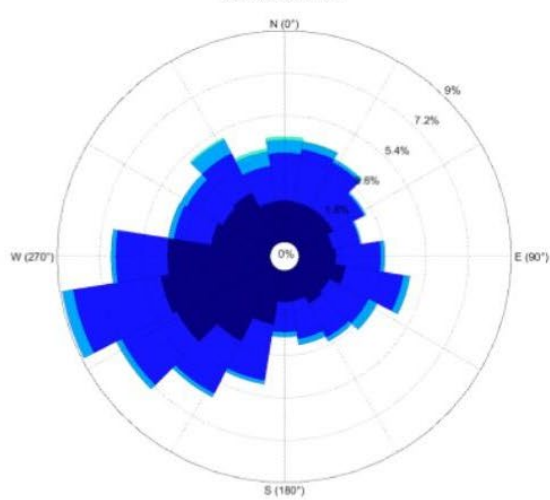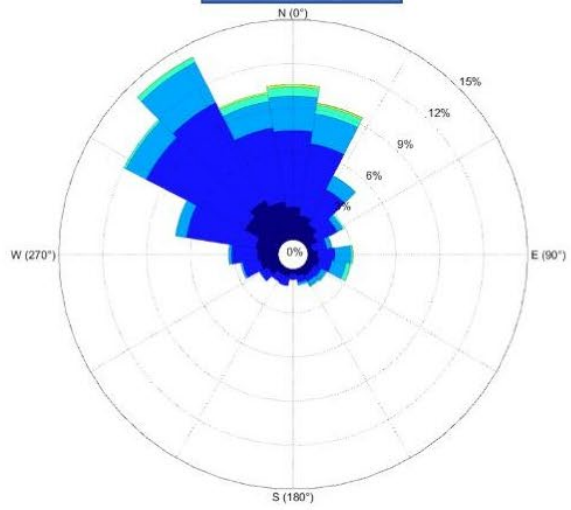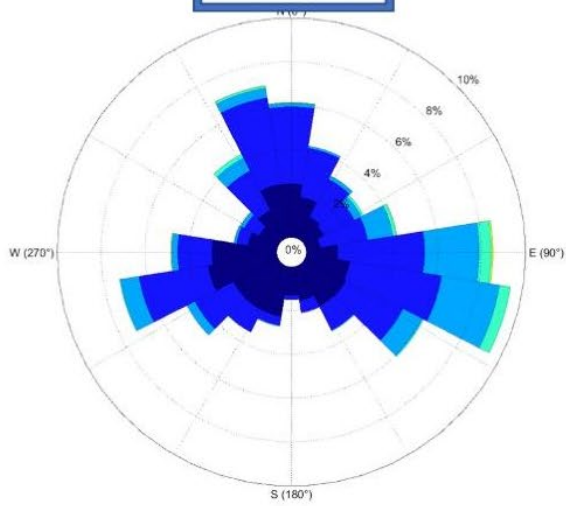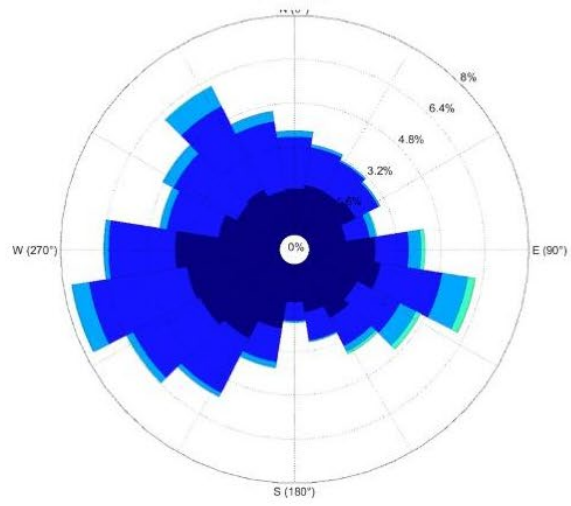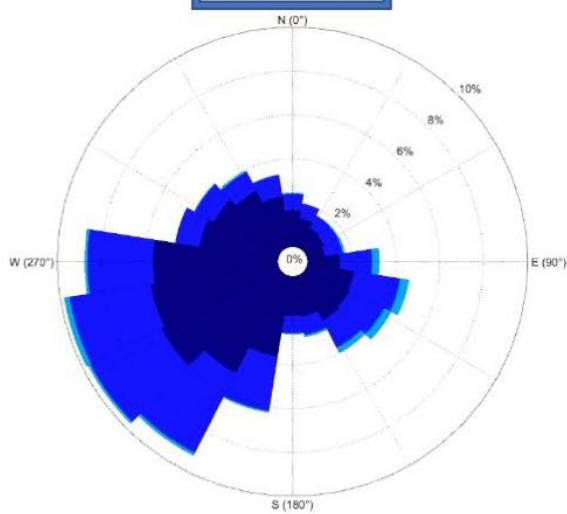
Period 18
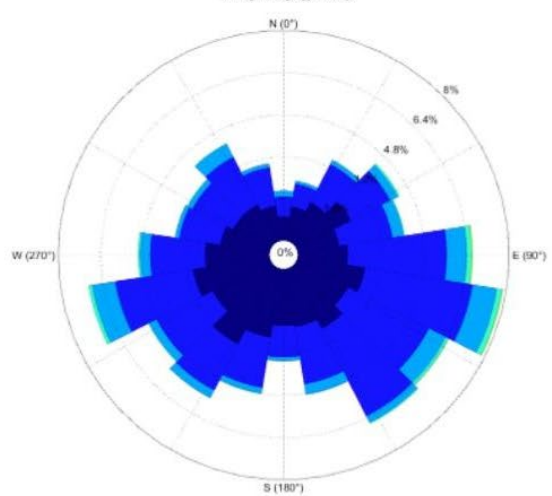
Period 19
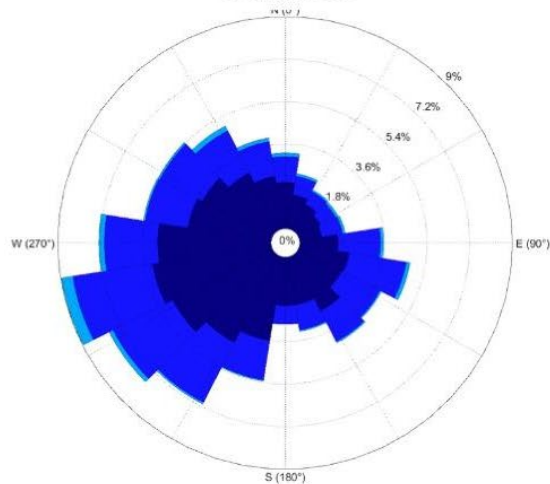
Period 20
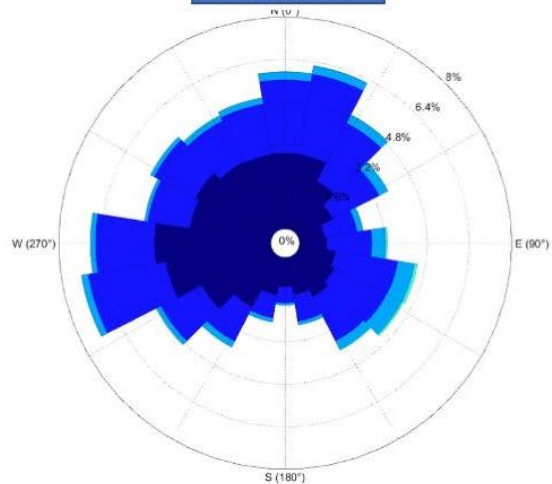
Period 21

Period 22

Period 23

Period 24

Period 25

Period 26